Dingley, D. J., Meaden, G., Dingley, D. J., & Day, A. P. (2018). A review of EBSD: From rudimentary on line orientation measurements to high resolution elastic strain measurements over the past 30 years. In *18th International Conference on Textures of Materials, ICOTOM 2017: Proceedings of a meeting held 6-10 November 2017, St. George, Utah, USA* [012003] (IOP Conference Series: Materials Science and Engineering; Vol. 375, No. 1). IOP Publishing. https://doi.org/10.1088/1757-899X/375/1/012003

A review of EBSD: from rudimentary on line orientation measurements to high resolution elastic strain measurements over the past 30 years.

A review of EBSD: from rudimentary on line orientation measurements to high resolution elastic strain measurements over the past 30 years.

David.J.Dingley[1] Graham Meaden[2] Damian. J. Dingley[3] and Austin P Day[4]
[1]H.H.Wills Physics Laboratory University of Bristol, UK
[2]BLG Productions Ltd., Bristol, UK.
[3]Vantage Software Inc., Salt Lake City, Utah, USA
[4]Aunt Daisy Scientific Ltd, Monmouth, UK.

Abstract. Considering that the Electron Back Scatter Diffraction technique, EBSD, features in more than 60% of the papers published in the current conference proceedings, this review concentrates on the most recent development in the last ten years, that is, High Resolution EBSD. An outline of the theory is presented and four-point bend test results are shown proving the sensitivity of the technique for measuring elastic strain is 1 part in 10000. Other examples of its use included here are strains surrounding indents in silicon, mapping the stress concentration at grain boundaries ahead of dislocation pile ups and dislocation generation at grain boundaries due to strain ahead of nano indentations. An application is presented to distinguish the c axis direction in slightly tetragonal PZT crystals and developments in obtaining absolute strain measurement as opposed to the relative strain measurement currently the norm are discussed.

1. Historical Note

The paper, 'On Line Microtexture Determination Using Backscatter Electron Kikuchi Diffraction in a Scanning Electron Microscope' was the first in which the EBSD technique was described at an ICOTOM meeting, Dingley 1987 [1]. In it the concept of direct crystal orientation measurement using a scanning electron microscope rather than the then universally used x-ray diffraction methods was presented. Now 30 years later, over 60% of the papers at the ICTOM meetings are applications of the EBSD technique and in excess of 1000 papers are published annually in which it is a major tool used in the investigation. The plenary lecture at the 1987 meeting by Professor Sir Charles Frank [2] was concerned entirely with orientation representation. He wrote "Thus, *because of the EBSD technique,* we now have a practical need for comprehensible displays of complete orientation statistics. To degrade that information to pole figures, showing the statistics of orientation of crystal planes, and not of crystals, is a criminal disregard of significant information." He would have been pleased then that although true orientation maps are not the normal method of orientation representation the alternative representation of the data in the form of inverse pole figure maps, Adams et al. 1993 [3] is so demonstrative that it has made EBSD a universally adopted tool in materials science.

The ICOTOM 1987 paper was one in a series starting with those of Prof. John Venables et al published between 1972 and 1977, [4]. On-line indexing evolved over the period 1983 to 1987 in the Bristol group lead by David Dingley [5]. Early enthusiasts using the Dingley system were Rolls Royce Bristol, UK, (M Parsley), National Physical Laboratory UK, (P Quested), SINTEF Norway (J Hjelen), Canadian Aluminium Company, Canada (E Balls), Universite Paris Sud, France, (R Pennelle), Nippon Steel, Japan (J Harase), Alcoa USA (H Weiland), Riso Denmark (D Juul Jensen and N-H Schmidt). However, the ICOTOM 1987 paper was particularly significant in that it lead directly to the development of what is known as Orientation Imaging Microscopy under the direction of Prof. Brent Adams and his team at

Yale University, Stuart Wright, David Field and Karsten Kunze with the author David Dingley as visiting professor, (1994), [3],[6] .

The main theme of the current presentation however, is not a review of the development of OIM over the succeeding 30 years as the standard EBSD technique is very well known, but to concentrate on the most recent advance, High Angular Resolution Electron Backscatter Diffraction, HREBSD. It is a tool developed principally at Oxford University in a materials group headed by Prof. Angus Wilkinson and provides quantitative data on internal strain, both the elastic strains and the dislocation distribution following plastic deformation. It is worth emphasising that these parameters, especially when mapped to show their spatial distribution, are of equal importance in materials characterisation as those of grain size, grain orientation, grain misorientation, grain boundary type and phase. A complete understanding of the origin of texture and its influence on mechanical properties and on behaviour during subsequent thermal mechanical treatment relies on knowledge of the entire microstructural description and the way it influences and is influenced by the strain and dislocation state. Some may have wished to include the energy state and its microstructural distribution in the list of essential microstructural features, but the energy state can be calculated form the stress strain data obtained from HR EBSD and as in one of the examples below it is implied in calculation of the von Mises parameter.

Standard EBSD does provide some semi quantitative data on strain. An early example is the image quality factor map, IQ map, as illustrated in figure 1, [7].

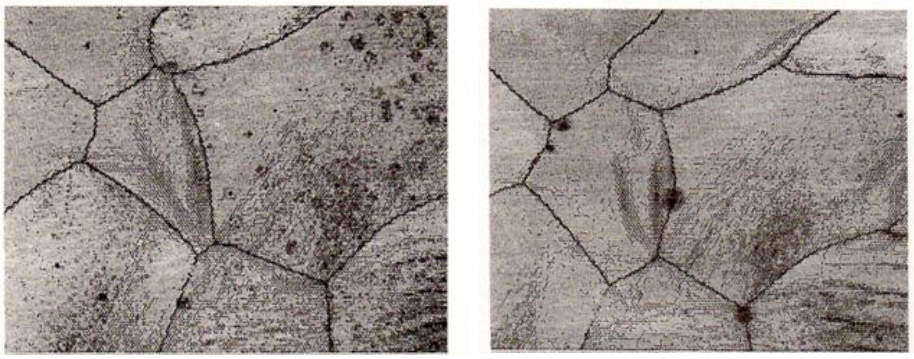

Figure 1. *Image quality maps of bcc iron adjacent to micro-hardness indentation. The second was recorded after polishing away a few microns of material.*

A more quantitative map is that of the kernel average map, KAM, originally included in the TSL commercial software.

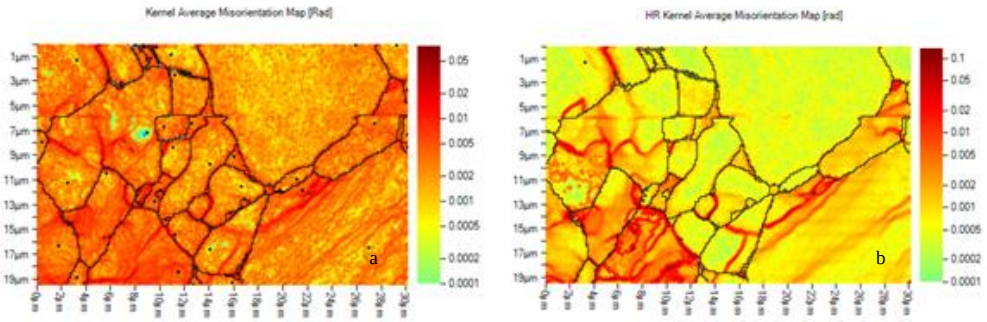

Figure 2, *kernel average maps a) standard EBSD, b) HR EBSD*

The KAM parameter is the value of the average misorientation between an element in a map with its nearest neighbours. An example map is shown in figure 2. The colour key is show on the right. For comparison a High Resolution KAM is shown alongside to demonstrate the improved angular sensitivity possible using the advanced technique.

2. The basis of HR EBSD

The basic point is that any crystal distortion caused by internal or insitu applied stress results in a corresponding distortion of the EBSD pattern. Zone axes shift in different directions and by different amounts according to the strain. At 0.2% strain, the strain at which yield stress values are often quoted, zone axes shifts in the direction of the applied tensile strain would be 2 parts in 1000. An elastic strain measurement tools needs to be ten times more sensitive. Although there had been a number of early publications exploring methods of determining this distortion, notably those by Wilkinson, reference [8] for example, the major step forward was published in 2006 by Wilkinson Meaden and Dingley [9] titled "High-resolution elastic strain measurement from electron backscatter diffraction patterns: New levels of sensitivity." The procedure is well detailed there and in many subsequent papers, e.g. [10] so that apart from some essential points most of the detail need not repeated here.

The Wilkinson method achieves the required level of sensitivity by using an image cross correlation procedure in which an EBSD pattern 'the test pattern' is correlated with a reference in the same grain. The reference pattern is nominally from a stress free region or one in minimal stress. The respective values for pattern centre coordinates PCx PCy and specimen to screen distance Z, for the two patterns have to be known with the same precision as that of the sort after strain sensitivity, though the absolute values can be in error by up to 1% of the screen diameter, [11]. Finding a suitable reference is straight forward, for example, in an indent in a silicon single crystal where the strain can be considered zero far from the indent and the relative positions of the PCx PCy Z values between reference and test points are known from the electron beam movement between the two patterns and the sample tilt. Finding a suitable reference point is less certain in other cases, in a deformed polycrystalline sample for example. Whatever the situation, the results for test points are always relative to the actual stress state of the point from which from which the reference pattern was taken.

Figure 3 illustrates the relevant geometry. On the left is a schematic of the distortion of an unstrained unit cell from cubic to skew. The vector **r** in the undistorted cell extends and rotates to form the vector **r'.** The displacement is the vector **Q**. To the right is shown the projection of this distortion onto the phosphor screen that images the EBSD pattern. The vector **Q** is projected as the vector **q.**

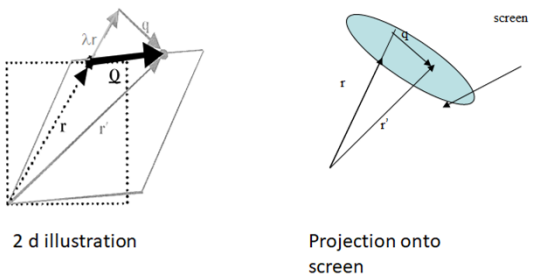

Figure 3. *Geometry relating lattice distortion vector **Q** to EBSD pattern distortion vector **q***

The two vectors are related by the equation

$$q = Q - \lambda r \qquad 1)$$

in which λ is a scalar of unknown magnitude.

The critical equations that describe the displacement are

$$zq_x - yq_z = (yz[a_{xx} - a_{zz}] + xza_{yx} + z^2 a_{yz} - xya_{zx} - y^2 a_{xy}) \qquad 2)$$

$$zq_y - xq_z = (xy[a_{xx} - a_{zz}] + yza_{xy} + z^2 a_{xz} - x^2 a_{zx} - xza_{zy}) \qquad 3)$$

In these equations x y z are the coordinates of the point r in the reference pattern, with respect to a coordinate system with origin at the pattern source point in the specimen. The quantities q_x q_y q_z are the respective vector displacements of the point r in the test pattern as measured in the phosphor screen. The crystal distortion components are a_{xx}, $a_{yy,}$ a_{zz}. There are 8 unknowns between the two equations. We thus need to make measurements on a minimum of four points in the pattern. In practice, instead of measuring the shift of individual points, a small region of interest, ROI, is drawn around each point and the average shift of all image elements within the ROI are determined. A cross correlation operation is used to do this and the average value found is assigned to the central point of the respective ROI. To reduce error and sampling problems many more than 4 ROI are selected and to improve the sensitivity to a fraction of a pixel a cubic spline procedure is included in the analysis.

If a non-symmetric deformation tensor is found from experiment this indicates rigid body rotation as well as strains are present. The deformation tensor is divided into its symmetric and asymmetric parts. The symmetric part is given by ½ $(A+A^T)$ which equals the strain tensor**.** The anti-symmetric part is given by ½$(A-A^T)$ which equals the rotation tensor. This provides the shear components e_{12} e_{13} e_{23} which because the strain tensor is symmetric are respectively equal to e_{21} e_{31} e_{31} . (Notation has changed here from subscripts xy etc, to subscripts 12 and the terms a_{xy} etc. to e_{12} to conform to accepted forms distinguishing a strain tensor from a distortion tensor). The rotation components are w_{12} w_{13} w_{23} which are respectively equal to $-w_{21}$ $-w_{31}$-w_{32}. The diagonal components of the strain tensor are only known at this stage as the differences $[e_{11} - e_{33}]$ and $[e_{22} - e_{33}]$ and 0. The term e_{33} can not be determined directly as the strain it represents is normal to the phosphor screen. However, noting that the free surface has zero traction across it, i.e. $\sigma_{33}= 0$ and using the generalized Hooke's law

$$\sigma_{ij} = \sum_{k=1}^{3} \sum_{l=1}^{3} C_{ijkl} \cdot e_{kl} \qquad 4)$$

where C is the fourth rank tensor defining the elastic constants for the material, we can write

$$C_{33}\, e_{33} + C_{13}\,(e_{11} + e_{22}) = \sigma_{33}=0 \qquad 5)$$

Using the appropriate substitutions we can solve separately for the three normal strains e_{11} e_{22} e_{33}.

Like all other metrics it is important to have an indication of the quality of the result. Two are used, geometric peak height of the cross correlation factor and the mean angular error. The

former measures to what extent, after beam shift and image zoom between reference and test patterns have been taken into account, the two EBSD patterns match. If the two patterns were both unstrained and there was no rotation between them then the correlation factor would be unity. If one were strained with only a small rotation between them the factor will be less but still close to unity. Factors as low as 0.6 might indicate a problem, e.g. a large rotation between the two patterns; one of the patterns had been degraded because of dirt on or damage to the sample surface, or because the beam shift and zoom correction values were in error. The latter is a likely occurrence if the distance between reference and test points on the sample exceed 300µm. This is because the SEM beam shift calibration can differ on day to day basis. The second cross correlation quality factor, the mean angular error, is calculated by taking the measured strain tensor and back calculating the pattern distortion that such a strain would produce in each of the ROI. The mean angular error is the angular difference between the back calculated distortion values and the experimental values.

3. Sensitivity.

It was shown in the 2006 WMD [9] paper that using an imaging camera with a sensor containing 1k x 1k pixels the cross correlation procedure could reliably detect a beam shift over the surface of a single silicon crystal of ±4µm, equivalent to ±0.1 of the size of one camera pixel or 0.001% of the screen width. The standard deviation was ±0.02pixels. This test has been repeated many times using different cameras with the ±0.1pixel level being the same no matter what the camera type. This means that a camera with a 2kx2k pixels sensor can detect a shift in the EBSD pattern twice as small and is clearly an advantage in HR EBSD work. The phosphor and aberrations of the imaging lens used in the system will of course also have an effect [12], but the values quoted are the best the author has measured. It follows that a map of the strain level for a scan over the surface of an unstrained region of a silicon crystal obtained using a 1kx1k camera should show no strain above the 1 to 2 parts in 10000 level. Figure 4, shows one such map, the shear strains e_{12}, demonstrating this point. The silicon crystal chosen had been deformed locally using a nano indenter. Whereas the strain surrounding the indent as seen in figures 4 a & b exceeds 0.005 it falls rapidly within a few microns. The reference EBSD pattern was recorded from a point 12µm from the indentation. It is at the top right of the map. The graph shows the e_{12} strain along the entire top line of the map, drawn as a blue line and from right to left. The red line shows the e_{12} strain down the last vertical column. The vertical column shows the strain is within 0.0002 of that of the reference pattern for 8 microns after which it rises as the strain from the indentation takes effect.

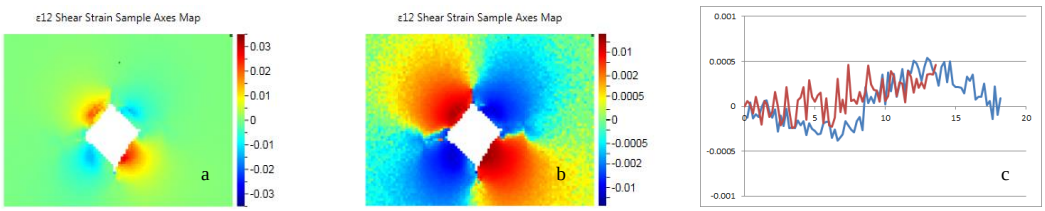

Figure 4, *a) e_{12} strain surrounding nano indent in silicon, linear scale, b) e_{12} strain with strain colouration according to a log scale, c) plots of e_{12} strains for the first row (right to left, coloured blue) and the last column (top to bottom, coloured red). (Data supplied by T Jaepel GmbH Dortmand).*

The horizontal row remains within 0.0002 strain of the reference point for 3 microns followed by a small negative shear and then a small positive shear. This proves that the reference point was truly in a region of zero strain and that the noise of the measurements, for the pixels close to the reference point, was within the 0.0002 limit claimed for the method.

4. Testing accuracy

The simplest experiment to verify that the technique can both accurately and precisely detect strain at a sensitivity comparable to that demonstrated above is the three point or four point bend test. The simplifying factor here is that the axis midway between the convex side and concave side of the bent sample is a neutral axis of zero strain and that the strain normal to the neutral axis increases linearly with distance from the axis. Thus selecting a reference point on this axis can confidently be assumed to be at zero strain. Figure 5a shows results from the work of Plancher et al [13][14]. The sample was stainless steel. The results shown are those Plancher obtained using a 1k x 1k EBSD camera, EDAX Digiview. EBSD patterns were recorded at 0.1µm intervals along the x axis as drawn in the figure. The data analysis was carried out using Crosscourt 4 software. The measurements were repeated by D. Loisnard and D. Dingley at EDF Moret-sur-Loing, using a 2k x 2k camera, Nordif HR4M, and the resulting strain variation is shown in figure 5b. Figure 5c shows an overlay of the results from the 2kx2k camera with those using micro Laue x-ray diffraction. All three data sets show the expected linearity of strain with distance from the neutral axis and the overlay shows exact correspondence of the data between the 2k x 2k camera result and the x-ray data. The noise level in the data from the 2k x 2k camera is half that from the 1k x 1k camera as also expected. The line profiles in figure 5c include the data collected outside the linear range in which the sample had deformed plastically. The EBSD data and x-ray data do not correspond perfectly in these regions as the line traces could not be set exactly in the same places for the two experiments.

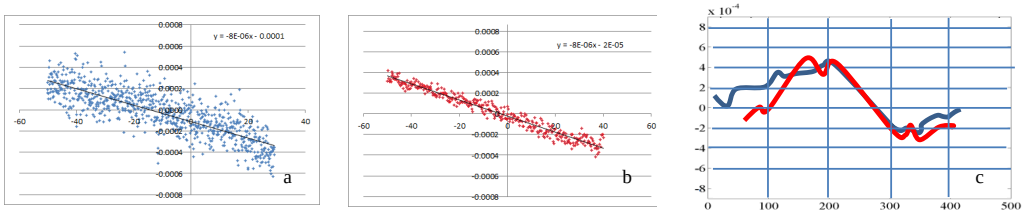

Figure 5, *a, Plancher data, b, Loisnard data and c, overlays of Loisnard data and micro x-ray data in which blue line is micro Laue and red HR EBSD.*

5. Relative rotations and geometrically necessary dislocations.

As explained above the ant-symmetric components of the off axis distortion tensor are a measure of the rotation of the point sampled in the experiment with respect to the orientation of the reference point. The relative rotations obtained have a precision of 0.006˚. This means IPF maps can be drawn with 100 times the sensitivity of those using the standard Hough measurements. The relative orientations as measured using cross correlation are transformed to absolute orientation measurements by adding to all the relative measurements the absolute orientation of the reference point as obtained using a conventional Hough transform or as outlined below using an improved high resolution Hough based measurement. Although the

so determined absolute measurements have the accuracy of the Hough measurement the relative orientations retain the 1 part in 10000 precision. This is important because the well-established Kernel Average Map used as a qualitative representation of plastic deformation retains the 100 times increased sensitivity available when calculated using cross correlation. The two Kernel Average maps shown in figure 1 demonstrate this difference and show that much of the data obtained using conventional Hough technique reflects its poor relative orientation measurement sensitivity.

The 0.006º precision however, also means that the strain gradient between points in a map can also be obtained at sufficient precision for a meaningful generation of maps displaying the distribution of the Geometric Necessary Dislocation (GND) density. A gradient precision of 1 part in 10000 allows for a GND density of 10^{12} to be detected, i.e. a dislocation spacing of 1 micron. The mathematical procedures involved can be found in the papers by Arsenlis and Parks, [15] and in the paper by Wilkinson and Randman [16]. The data shown here in figure 6b was obtained using the Wilkinson Randman approach in software supplied by BLG Vantage (CC4). In figures 6 a, b and c are shown a correlation between the maximum principal strain value, the GND density distribution and the stress value normal to the grain boundary between the points marked x-x. The sample was tantalum with nanoindents at regular distances from the grain boundaries. Data supplied by courtesy of B Dunlop, Mitchigan State University.

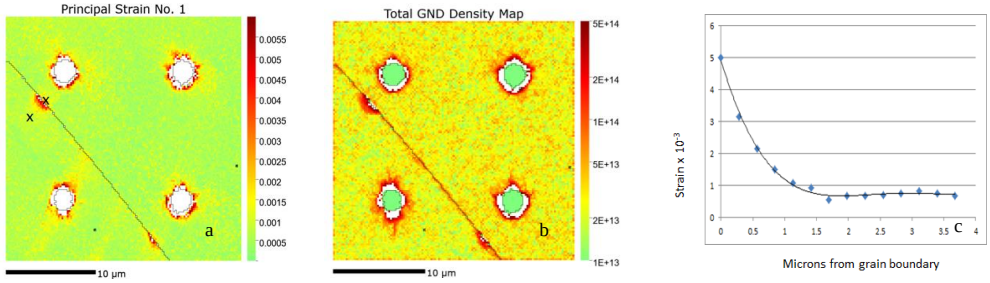

Figure 6. *a, Principal strain map surrounding nano indentations, b corresponding total GND density map, c, strain versus distance from grain boundary between points x x . (With acknowledgements to Bret Dunlap Michigan State University).*

6. Antiphase boundaries.

The high precision achieved by the method also permits a novel method for determining the presence of antiphase boundaries. Consider for example a PZT sample in the unpolarised state. The crystal is naturally tetragonal but the c to a ratio is often too small,~1.02, for conventional EBSD to distinguish the <100> axis from the <001> axis. However, this is well within the detection limit of HR EBSD. It is not possible though, to use the strain algorithm as described above as the tetragonality is not caused by strain but is simply because of the crystal class. Hence, to distinguish the c from the a b axes (a=b in this case) the procedure differs slightly. A reference point as selected as normal within a grain and the distortion between the reference pattern and a test pattern carried out as described above. We know from the crystal system that the crystal extension is along one of the 100 type axes. As the tetragonality is small we can at first treat the crystal as though it were cubic. We can thus determine its orientation using the Hough transform and find the real space directions of the 001 type axes. Figure 7 shows two domains in the PZT microstructure oriented at 90º to each

other. The extension of the c axis is exaggerated to clarify the argument. The real space directions for these axes are labelled x y and z in the figure. The problem is to determine which of the crystal axes parallel to x y z is the longest. We next need to consider the initial output of the distortion tensor. As discussed following equations 2 & 3 the output from the cross correlation procedures gives us x distortion = [e_{11}–e_{33}], y distortion = [e_{22}–e_{33}] and z= 0. If we view the example shown in figure 7, which is one of the three possible orientation relationships between two disorientated domains in PZT, we see that the pattern from the test point compared with that from the reference point will show a shortening only in the x reference direction. From the figure the shortening is a-c. This is equivalent to a strain e_{11}. Along the z reference direction the change is c-a= e_{33}. Hence [e_{11} –e_{33}] which is equal to the x component of the distortion tensor =2(a-c). Similar arguments for the changes [e_{22}–e_{33}] show that this difference =a-c, half that for the former. Thus, as shown in the inset to figure 7, for a tetragonality of 2.7%, the x axis will show a distortion of -0.054, the z axis, a contraction of -0.027 with no change in the y direction. Thus the c axis of the reference pattern is parallel to x and that of the test pattern parallel to z. The other two possible domain orientation relationships provide different values along the x y and z reference directions. Hence it is possible to distinguish for all three domain orientation relationships along which of the x y z real space directions the c axis lies. Figures 7b and c are two HR EBSD maps showing these measurements on a selected grain. The black arrows are the surface projections of the measured real space 100 type directions.

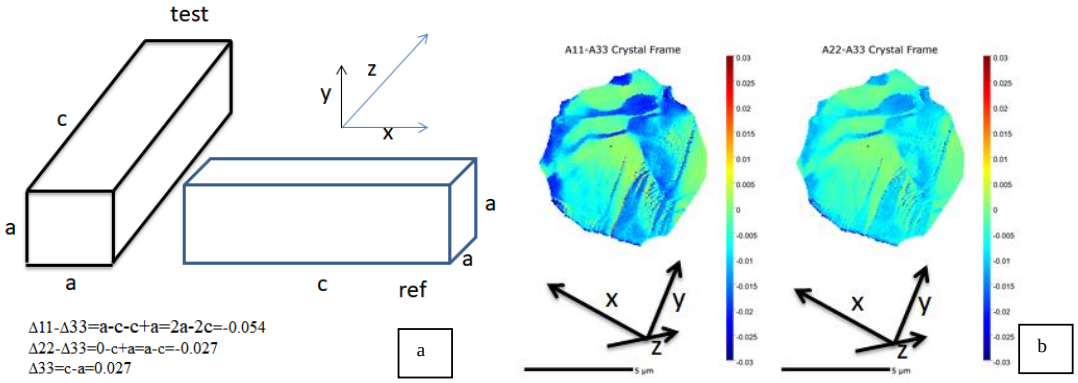

Figures 7 *a) schematic of domain orientations, b), the dark blue regions are the [001] domains, the light blue and green regions are the {001} domains.*

From the schematic and the attached analysis, which is for test point minus reference, the darker blue pixels in 7b correspond to the lattice parameter parallel to the x axis being shorter than that in the reference crystal. The [001] axis of the reference point, shown as a black dot in the green central grain is parallel to the X axis in the map. Similarly it can be deduced that the [001] axis in the dark blue regions is parallel to the Y axis in the map. In the particular example shown the domains are also under elastic strain so that the actual measurements for a particular orientation will show a variation in the values [e_{11}–e_{33}] and [e_{22}–e_{33}] hence the small deviations in blue and green colours shown in the map within domains in the same orientation.

7. Absolute strain measurement

The Wilkinson cross correlation procedure for measurement of residual strain provides values relative to the strain state of the point in the sample used to obtain the reference pattern.

Though the measurement of strain distribution and relative strain between points remains a valid and powerful addition to microstructural characterisation as illustrated in figure 5; obviously it fails in providing absolute, i.e. true strain, stress and if required energy values. For example the maximum strain ahead of the grain boundary as shown in figure 5c is given as 0.005 but this is relative to the measured background strain truly being at the 0.0008 level. There are two ways the uncertainty in the strain of the reference point might be overcome; by the use of simulated EBSD pattern as the reference pattern in place of a real pattern, or by improving the sensitivity and accuracy of Hough based analysis. The use of simulated patterns has been explored over the past 8 years beginning with Kacher et al [17] who used kinematical diffraction theory to calculate the intensity distribution for different reflections. Maurice et al [18] showed soon after that such simulations based on kinematical theory lead to false results. Dynamical theory calculations produce much better correspondence with real patterns,. These simulations, beginning with the work of Winkelmann [19], have improved the situation and recently Alkorta et al [20] have reported that further improvements in the correspondence can be achieved by using the differential of both the real and simulated patterns as input to the cross correlation procedure. These latter papers have concentrated on the problem that it is imperative for the pattern centre and specimen to screen values used to generate the simulation have to be the same as the values in the test pattern. As the experimental values are not know better than 1% to 2% of the screen diameter, then an iterative procedure needs to be followed to find exactly identical values. This might be possible if the sample pattern was from an unstrained point in the crystal for example. Doing the same for a test point in the crystal that is of unknown strain and uncertain orientation considerably magnifies the problem. Figures 8a b & c illustrate the matching problem. The real EBSD pattern in 8a is from germanium. The simulations 8b 8c, were provided by Aunt Daisy Scientific. The Hough based values for PCx PCy and z and crystal orientation were those used for computing the simulations

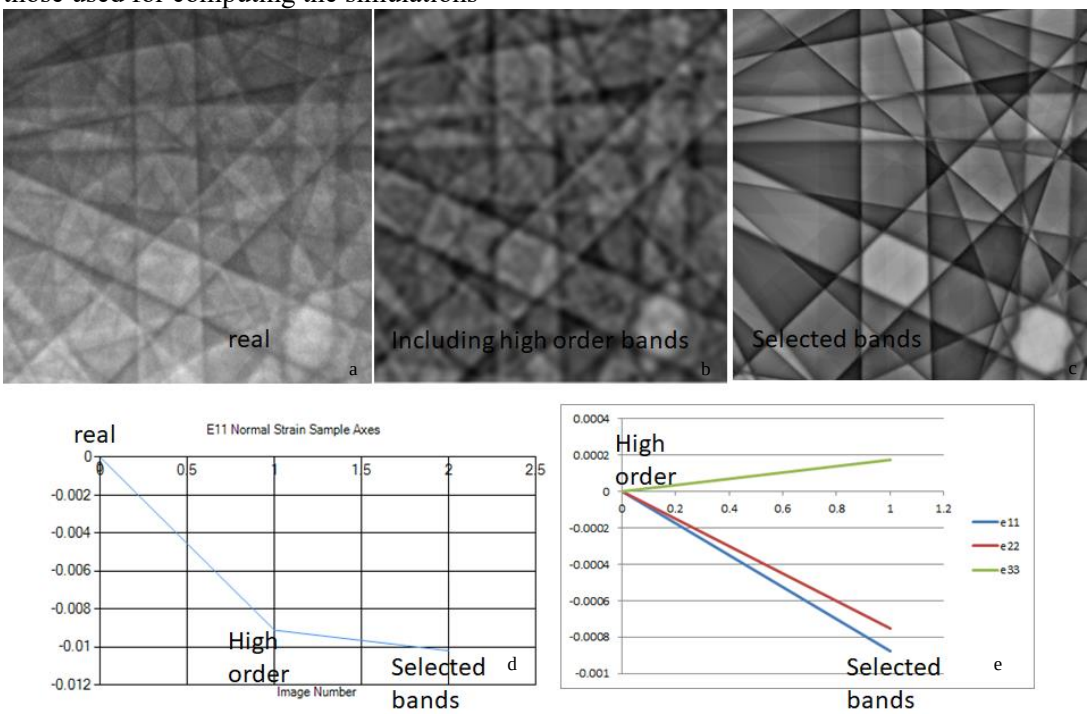

Figures 8 a)EBSD pattern from Ge at 2kx2k resolution, b) dynamic simulation at same resolution with large number of reflectors used in the computation, c) dynamic simulation

using limited number of reflectors, d) e_{11} strain values using real pattern as reference, e) normal strain values for pattern c using simulated pattern, b, as reference pattern.

Figure 8a is the real pattern; 8b is a simulated pattern using a large number of reflectors and 8c a simulated pattern using only bands seen in the real pattern. The two simulated patterns were cross correlated first against the reference pattern and then pattern 8b was used as reference for cross correlation with pattern 8c. Figure 8d shows the e_{11} strain as measured for the 3 patterns. Figure 8e is a plot of the e_{11} e_{22} e_{33} strains of pattern 8c with respect to pattern 8b used as reference. The data in figure 8e indicates that even when the PC x y & z coordinates (as well as the orientation) are the same, the cross correlation can fail to give the correct answer, zero strain in this case. The error in e_{22} and e_{33} show strains of almost 0.0008. They can only be due to differences in the number of bands used in the simulations. The large difference in apparent strain values (figure 8d), when the real pattern 8a is cross correlated against the simulated patterns, is a combination of insufficient correspondence between real and simulated patterns as well as the PC x y z values of the simulated patterns not being the same as the real pattern. Which of the two simulated patterns best fits the quality of the real pattern and whether either are sufficiently similar to the real pattern to provide reliable cross correlation data is open to question. We leave the arguments of using simulations to determine the strain state as still a very open ended problem.

The advent of a Nordiff HR4M high resolution camera of 2050x2050 pixels with 12 bit deep images as currently used at the EDF laboratory, Moret-sur-Loing, has encouraged a re-examination of using Hough type analysis of the EBSD pattern to improve its sensitivity. Figure 9 shows a detail of an HR EBSD Hough peak obtained from analysis of one such EBSD pattern a germanium crystal.

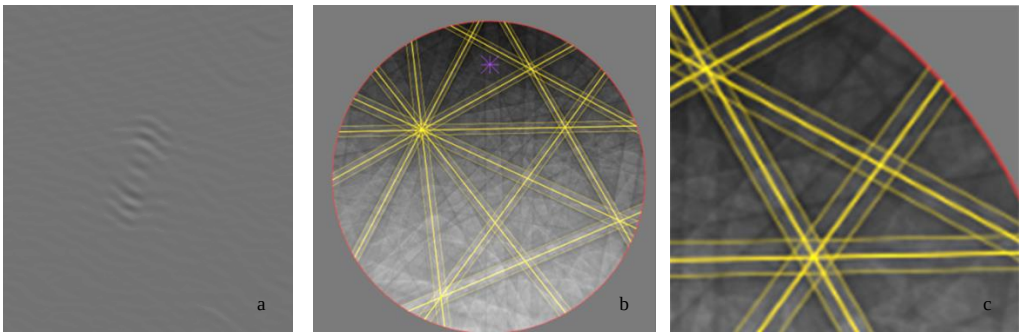

Figure 9, *a) Hough peak for [220] and higher order reflections, b) superimposed band edges as found from Hough analysis, c) detail of part of overlay.*

In Hough space (9a) the vertical axis is the normal distance ρ, from the EBSD pattern centre to a straight line drawn through the EBSD pattern. The horizontal axis is the inclination, θ, of that line. At high resolution, the transform highlights the Kikuchi band edges in the pattern rather than the band itself. The detail is for the 220 reflection and shows three orders of reflections. The straight lines that are tangential to the hyperbola give rise to the dark and bright regions in Hough space. The angular change between tangents at the highest resolution is 5×10^{-4} radians. When the tangent point in the EBSD pattern passes through the point where the vector defined by ρ, θ is shortest possible for each Kikuchi line bordering a Kikuchi band, the shape of the Hough peak shows an inflection. This is clearly seen in the figure. The Kikuchi band edges on the opposite sides of the bands produce intensity profiles in the

Hough plot which are the inverse of each other. This is due to an asymmetry in the diffracted intensities which is a function of the tilt of the sample with respect to the incident beam. The intensity difference is zero for reflections that are normal to the tilt axis and maximum for those parallel to it. The geometric mid-point in Hough space between the Hough inversion points corresponding to either side of the Kikuchi band, defines the rho value corresponding to the centre line of the Kikuchi band. The normal to this line passing through the mid-point also passes through the true pattern centre. (It leads to a better determination of the PC position as will be explained in a coming publication). The centre line of the Kikuchi band is 7the line defining the intersection of the projection of the diffracting plane onto the phosphor screen. Thus, careful analysis of all Hough peaks permits the rho theta values of the centre lines of all Kikuchi bands to be determined. In addition because of the higher resolution used in the analysis and also the method of interpreting the Hough peak, the accuracy and precision is greater than in conventional Hough applications. Hence, measurement of interplane angles and consequent orientation determination is also improved. Figure 9b shows an overlay of the found band edges on the original EBSD pattern for all pairs of bands. The important features to observe are the intersection points of the centre bands for three intersecting bands. In the detail shown in figure 9c, two such intersections are shown. If the result were perfect the centre lines would intersect at a point. In one case this is true but in the other the splitting is calculated as just 2 pixels in 2000.

8. Conclusions

Thirty years of EBSD at ICOTOM has seen a transition from a rudimentary procedure for on-line determination of crystal orientation in the SEM, to a technique that can now acquire data at a rate approaching one thousand patterns a second and produce maps relating all the major factors affecting the physical properties of the material. The growth of applications has been remarkable, but yet there are still areas that require further development and enhancement. In this paper the most challenging application, that concerned with the measurement of elastic strain and local rotation gradients, both at the 1 part in 10000 level, has been reviewed in detail. The claimed precision has been proven for relative measurements with respect to a pattern obtained from a reference point in the sample. Absolute measurement remains a challenge with two possible approaches; that of using a computer simulation as the reference pattern and that of improving the accuracy of measurement of interplanar angles using a high resolution Hough procedure, are part of an ongoing investigation.

9. Acknowledgements

The author would like to acknowledge that the advancement of EBSD in materials research following the first publication at an ICOTOM meeting would not have happened without the contributions in particular from, Prof Brent Adams, Prof. David Field, Dr. Stuart Wright, Dr. Karsten Kunze, Matt Nowell Dr. Krieger Larsen and more recently by Prof. Angus Wilkinson and Dr. Ben Britton.

10. References

[1] Dingley D J 1987 On line microtexture determination using backscatter Kikuchi diffraction in a scanning electron microscope, Eighth International Conference on Textures of Materials (ICOTOM 8) (The Metallurgical Society) ed. J S Kallend and G Gottstein 189-194
[2] Frank C 1987 Orientation Mapping, Ibid

[3] Adams B L Wright S I and Kunze K 1993 Orientation imaging: The emergence of a new microscopy. *Metallurgical Transactions A* **24**(4): 819-831
[4] Venables J A and Bin-Jaya A 1977 Accurate micro-crystallography using electron backscatter diffraction. *Phil Mag.* **35** (5) 1317-1332
[5] Dingley D J, Alderman J, Longden M and Weinbren J, 1987 Online analysis of electron back scatter diffraction patterns 1. Texture Analysis of Zone Refined Polysilicon." *Scanning Microscopy* **1**(2) 451-456
[6] Adams B L, Dingley D J, Kunze K and Wright S I' (1994). "Orientation Imaging Microscopy: New Possibilities for Microstructural Investigations using Automated BKD Analysis." *Materials Science Forum* **157-62**: 31-42
[7] Dingley D J and Kunze K (1994) Orientation imaging Microscopy and serial sectioning, ICEM Paris *Les editions de physique* editing B Jouffrey and C Colliex **2B** 1313-1314
[8] Wilkinson A J, 1996 "Measurement of elastic strains and small lattice rotations using electron back-scatter diffraction." *Ultramicroscopy* **62**(4): 237-247
[9] Wilkinson A J, Meaden G and Dingley D J' 2006 "High-resolution elastic strain measurement from electron backscatter diffraction patterns: New levels of sensitivity." *Ultramicroscopy* **106** (4-5): 307-313
[10] Dingley D J, 2016 High angular resolution EBSD for measurement of strain and residual dislocation density. *EBSD: Analyse par diffraction des electrons retrodiffuses,* Groupement National de Microscopie Elecronique, edit. Francois Brisset
[11] Villert S, Maurice C, Wyon C and Fortunier R. (2009) Accurate assessment of elastic strain measurement by EBSD, *Jounal of Microscopy* **233** 290-301.
[12] Mingard K, Day A., Maurice C, and Quested P N, (2011) Towards high accuracy calibration of EBSD systens. *Ultramicroscopy* **111** 320 329
[13] Plancher E, 2015 Mesures de champs de deformations elastique et totalepour la determination du comportement mecanique local de materiaux cristallins. Doctorat ParisTech l'École Nationale Supérieure d'Arts et Métiers
[14] Plancher E, Favier V, Maurice C, Bosso E, Rupin N, Stodolna J, Loisnard D, Marijon JB, Petit , Micha J-S, Robache O and Castelnaua O, (2017) Measurement of local constitutive relations at the micrometre scale, in bulk metallic alloys, *J. Appl. Cryst*. **50**, 940–948
[15] Arsenlis A, Parks D M, Becker R and Bulatov, V, (2004) "On the evolution of crystallographic dislocation density in non-homogeneously deforming crystals." *Journal of the Mechanics and Physics of Solids* **52**(6): 1213-1246
[16] Wilkinson A J and Randman D, (2010). "Determination of elastic strain fields and geometrically necessary dislocation distributions near nanoindents using electron back scatter diffraction." *Philos. Mag.* **90**(9)
[17] Kacher J H, Landon C, Adams B L and Fullwood D, (2009) Bragg's law diffraction simulations for electron backscatter diffraction analysis, *Ultramicroscopy* 109 (9) (2009) 1148–1156.
[18] Maurice C, Fortunie R, Driver J, Day A, Mingard J A K and Meaden G, (2010) Comments on the paper Bragg's law diffraction simulations for electron backscatter diffraction analysis by Josh Kacher, Colin Landon, Brent L. Adams & David Fullwood, *Ultramicroscopy* **110** 7.
[19] Winkelmann A, Trager-Cowan C, Sweeney F, Day A P, Parbrook P, (2007) Many-beam dynamical simulation of electron backscatter diffraction patterns, *Ultramicroscopy* 107 (4–5) 414–421.
[20] Akorta J, Marteleur M, Jacques P J, (2017) Improved simulation based HR EBSD procedure using gradient-based DIC techniques, *Ultramicroscopy* **182** 17-27